

First law: the internal energy U of a system is a function of state that is changed only by heat flow or work done on the system:

$$\Delta U = U_2 - U_1 = q + w \quad (1)$$

$$w = - \int_{V_1}^{V_2} P dV \quad (2)$$

PdV is the pressure-volume work done by the gas when it expands by a volume change dV against a pressure P . The minus sign makes this the work done on the gas during such an expansion and the integral computes the total work going from one volume to another.

The change in U of the gas during the compression from V_1 to V_2 is the sum of the work in Eqn. 2 and whatever heat is allowed to flow. Suppose that no heat is allowed to flow into or out of the gas during the compression (a system that does not exchange heat with its environment is called *adiabatic*). In this case, the pressure and volume of an ideal monoatomic gas follow the rule $PV^\gamma = c$, where c is a constant and $\gamma=5/3$. Using this rule, the work done in compressing the gas is

$$w = - \int_{V_1}^{V_2} \frac{c}{V^{\gamma-1}} dV = \frac{c}{\gamma-1} \left(\frac{1}{V_2^{\gamma-1}} - \frac{1}{V_1^{\gamma-1}} \right) \quad (3)$$

and $\Delta U = w$ in this case, since $q=0$.

Second law: the entropy S of a system is a state function which changes with heat flow as

$$\Delta S = S_2 - S_1 = \int_1^2 \frac{dq}{T} \quad (5)$$

by a reversible process. For an irreversible process, the entropy change is greater than the integral above.

Deriving the Nernst equation:

$$\mu_i = \mu_i^0 + RT \ln C_i + z_i F V + \dots$$

Directly writing the condition for equality of electrochemical potential across the membrane gives:

$$\mu_i^0 + RT \ln C_1 + z_i F V_1 = \mu_i^0 + RT \ln C_2 + z_i F V_2 \quad (14)$$

Note the assumption that μ_i^0 is the same in both solutions. This should be true if the solutions differ only in ion concentration and electrical potentials. Canceling common terms and rearranging Eqn. 14 gives the Nernst equation:

$$V_2 - V_1 = E_i = \frac{RT}{z_i F} \ln \frac{C_1}{C_2} \quad (15)$$

In an aqueous solution, the interactions of solute and solvent molecules result in transport processes being limited largely by the equivalent of frictional forces; there are no elastic forces restraining an ion in a liquid solution (i.e. no little springs restricting an ion to certain positions) and the frictional forces turn out to be larger than inertial ($f=ma$) forces. Thus when an ion is acted on by an electric field, it tends to move with a *drift velocity* that is proportional to the force provided by the field. This assumption is motivated by the usual behavior of friction, in which the force needed to overcome friction is proportional to the velocity. The *mobility* u_i of an ion is the ratio between the drift velocity and the applied force. That is,

$$\left(\begin{array}{l} \text{drift} \\ \text{velocity} \end{array} \right) = u_i \times (\text{force / mole}) = -u_i z_i F \frac{dV}{dx} \quad (17)$$

where u_i has units (m/s)/(N/mole). In some texts, mobility is defined as the electrical mobility, the ratio of drift velocity to the quantity $z_i dV/dx$.

The flux J_i of the ion is the number of moles of ion passing through a unit area per second and is given by $J_i = C_i u_i z_i F$ (drift velocity). Thus the ion flux driven by an electric field is

$$J_i = -u_i C_i z_i F \frac{dV}{dx} \quad (18)$$

Net flux can also be produced in solution by concentration gradients, as described by Fick's law:

$$J_i = -D \frac{dC_i}{dx} \quad (19)$$

Fick's law can be derived from a consideration of the effects of random thermal motion of particles in a concentration gradient.

The net flux in solution is then the sum of Eqns. 18 and 19. Usually the expression is simplified by noting that $u_i RT = D$ (Einstein relationship, see Feynman, pp. 43-8 for a derivation). The result is the *Nernst-Planck equation*.

$$J_i = -u_i \left[RT \frac{dC_i}{dx} + C_i z_i F \frac{dV}{dx} \right] = -u_i C_i \left[RT \frac{d \ln C_i}{dx} + z_i F \frac{dV}{dx} \right] \quad (20)$$

minus the potential outside and current is positive in the outward direction. The Nernst-Planck equation in terms of current density, with the reversed sign convention, is

$$I_i = z_i F u_i C_i \left[RT \frac{d \ln C_i}{dx} + z_i F \frac{dV}{dx} \right] \quad (21)$$

The steady-state assumption implies that flux J_i and the current density I_i are constant in the membrane, not functions of x . To see this, consider Fig. 7 which shows the flux at two points x and $x+dx$ in the membrane. The total amount of ion in a unit area between x and $x+dx$ is $C_i(x)dx$ and the time rate of change of this amount is the difference between the flux into this region and the flux out.

$$\frac{\partial(C_i dx)}{\partial t} = J_i(x) - J_i(x+dx) \quad (22)$$

Dividing through by dx and taking the limit as dx goes to zero,

$$\frac{\partial C_i}{\partial t} = -\frac{\partial J_i}{\partial x} \quad (23)$$

Now in the steady state, $\partial C_i / \partial t = 0$ so that $\partial J_i / \partial x = 0$ also; thus in the steady state, the flux, and the current density I_i are constant, independent of x .

Now Eqn. 21 can be rearranged and integrated through the membrane as follows:

$$I_i \int_0^d \frac{dx}{z_i^2 F^2 u_i C_i} = \frac{RT}{z_i F} \int_0^d \frac{d \ln C_i}{dx} dx + \int_0^d \frac{dV}{dx} dx \quad (24)$$

Current density I_i has been taken out of the integral on the left-hand side because of the steady state assumption. The integrals on the right hand side can be evaluated, giving

$$I_i \int_0^d \frac{dx}{z_i^2 F^2 u_i C_i} = \frac{RT}{z_i F} \ln \frac{C_i(d)}{C_i(0)} + V(d) - V(0) \quad (25)$$

which can be written in the form

$$I_i R_i = \Delta V - E_i \quad (26)$$

where R_i is the integral on the left hand side of Eqn. 25, ΔV is the transmembrane potential ($V(d) - V(0)$), and E_i is the equilibrium potential for the ion (Eqn. 15).

Eqn. 26 is just a statement of Ohm's law for electrical circuits; it shows that the Nernst-Planck equation is equivalent to the following electrical model for current flow through a membrane:

The diffusion potential

Eqn. 21 can be integrated in a different way, again for the situation in Fig. 6; this integration will yield useful information about current-voltage relationships and membrane potentials in two special cases. Note that

$$\frac{d}{dx} \left[C_i e^{-z_i F V / RT} \right] e^{z_i F V / RT} = \frac{dC_i}{dx} + C_i \frac{z_i F}{RT} \frac{dV}{dx} \quad (27)$$

so that Eqn. 21 can be rewritten as follows

$$\begin{aligned} I_i &= z_i F u_i RT \left[\frac{dC_i}{dx} + C_i \frac{z_i F}{RT} \frac{dV}{dx} \right] \\ &= z_i F u_i RT \frac{d}{dx} \left[C_i e^{-z_i F V / RT} \right] e^{-z_i F V / RT} \end{aligned} \quad (28)$$

Integrating Eqn. 28 through the membrane gives,

$$I_i \int_0^d e^{-z_i F V / RT} dx = z_i F u_i RT \int_0^d \frac{d}{dx} \left[C_i e^{-z_i F V / RT} \right] dx \quad (29)$$

The current density has been taken out of the integral because of the steady state assumption. The right hand side can be evaluated, giving an expression for the current-voltage relationship for the ion.

$$I_i = z_i F u_i RT \frac{\left[C_i(d) e^{-z_i F \Delta V / RT} - C_i(0) \right]}{\int_0^d e^{-z_i F V / RT} dx} \quad (30)$$

The constant-field equation

Frequently it is assumed that the membrane potential is a linear function of distance through the membrane (as drawn in Figs. 6, 9 and 11). While this can be shown to be true in one special case (see Question 14), it is at best an approximation in most cases. Nevertheless, it provides a

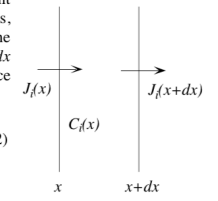


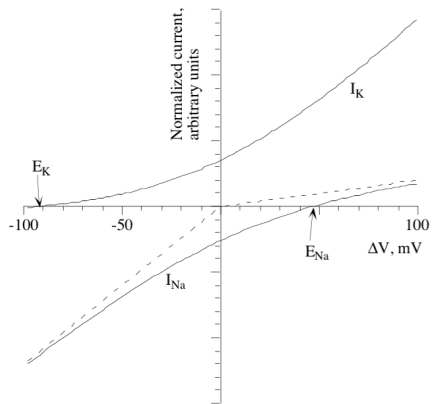
Figure 7: Relationship of fluxes and concentration at two points in the membrane.

useful approximation for many membrane currents. With the assumption that $V(x)=\Delta Vx/d$ for $x=[0,d]$, the integral in the denominator of Eqn. 30 can be evaluated, giving the *constant-field equation*:

$$I_i = \frac{(z_i F)^2 u_i}{d} \Delta V \frac{[C_i(d) e^{z_i F \Delta V / RT} - C_i(0)]}{e^{z_i F \Delta V / RT} - 1} \quad (35)$$

Figure 12. Current-voltage plots for sodium and potassium using the constant-field theory.

Fig. 12 shows a plot of constant-field currents I_K and I_{Na} against membrane potential ΔV , for the ion concentrations listed in Question 5. Note that the currents go to zero at the equilibrium potentials, as expected. The current-voltage curves are nonlinear; this nonlinearity is called *rectification*. The sodium current is larger for inward currents (negative), called *inward rectification* and the potassium current is the opposite, *outward rectification*. The origin of the rectification in this case is the difference in intracellular and extracellular concentrations. Essentially, the outward current for $\Delta V > E_i$ is supplied by the intracellular concentration and vice versa. Thus the current will be outward rectifying (like potassium) if the ion concentration is higher inside than outside the cell.



Nature of the cellular steady state

The models considered above, the means by which concentrations gradients are set up and maintained was ignored. Of course, in a real cell, there must be active transport mechanisms to maintain the ions out of equilibrium. A variety of mechanisms have been described (see Läuger, 1991 for a complete description). The most common mechanisms in neurons include Na-K-ATPase, which transports sodium and potassium against their electrochemical potential gradients (Na out of the cell, K into the cell) using ATP hydrolysis as the energy source (Question 9); Ca-ATPase, which does the same for calcium; and the Na-Ca exchanger, which transports calcium out of the cell using the energy in the sodium electrochemical potential.

In the presence of active transport, the nature of the steady state equations used above (Eqns. 31 and 37) is different. For each ion in the system there must be both an active transport I_i^A and a passive transport I_i^P . The passive transport is described by the flux equations developed above (i.e. Eqns. 30 and 35). For similar models of active transport, see Läuger (1991). In the steady state, the ion's concentrations must be constant, so that the net flux of ion through the membrane must be 0, $I_i^A + I_i^P = 0$. If this equation holds for every ion in the system, then there can be no net flux of any ion through the membrane and the net charge transfer through the membrane is guaranteed to be zero. Looking at the system this way, Eqns. 31 and 37 do not capture the true nature of the steady state.

Apparently the true steady state in a cell is a more complex situation than has been considered in deriving the traditional diffusion-potential models above (Eqns. 33 and 38). A natural question is why these models apparently work for data from real cells, given the inaccuracy in the assumptions that underlie them. One special case in which active transport can be included in the membrane-potential model occurs when only sodium and potassium are permeable through the membrane by passive transport. Their concentrations are maintained by active transport through Na-K-ATPase. A characteristic of this enzyme is that 3 Na ions are transported for each 2 K ions. The steady state equations then become:

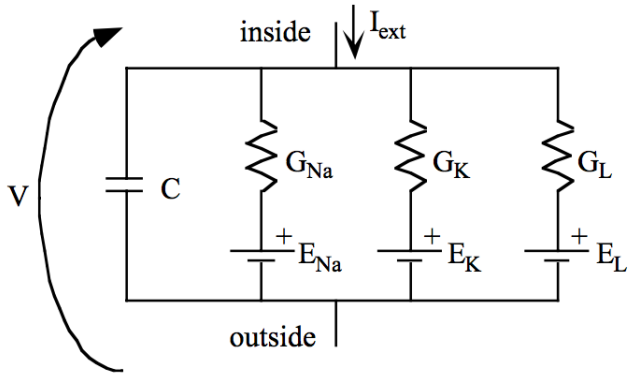


Fig. 1 Typical membrane circuit containing active Na and K channels, a leakage channel and a membrane

$$C \frac{dV}{dt} = I_{ext} - G_{Na}(V - E_{Na}) - G_K(V - E_K) - G_L(V - E_L)$$

$$G_{Na} = \bar{G}_{Na} m^3 h \quad \frac{dm}{dt} = \frac{m_\infty(V) - m}{\tau_m(V)}$$

$$\frac{dh}{dt} = \frac{h_\infty(V) - h}{\tau_h(V)}$$

$$G_K = \bar{G}_K n^4 \quad \frac{dn}{dt} = \frac{n_\infty(V) - n}{\tau_n(V)}$$

$$m_\infty(V) = 0.5 [1 + \tanh((V - V_1)/V_2)]$$

$$n_\infty(V) = 0.5 [1 + \tanh((V - V_3)/V_4)]$$

$$\tau_w(V) = \frac{1}{\cosh((V - V_3)/V_4)}$$

Fig. 2 Parameters of the Hodgkin-Huxley model for squid giant axon membrane.

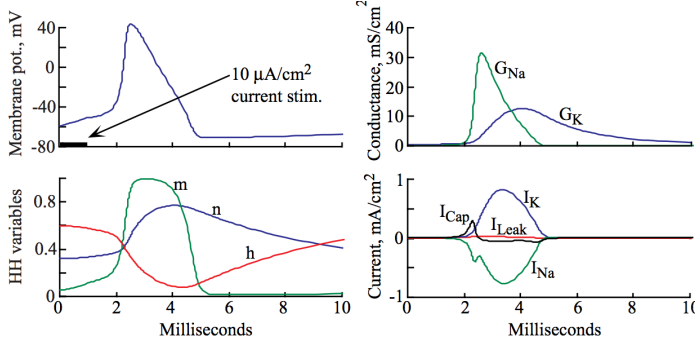
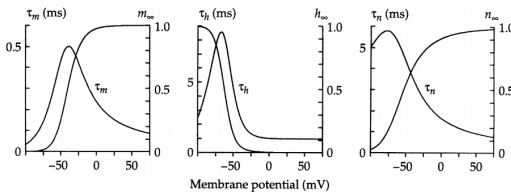


Fig. 3 Time course of the important variables in the HH model for nerve action potentials during an action potential. Shown are the membrane potential (upper left), the HH variables (lower left), the conductances (upper right), and the membrane currents (lower right).

- For an increasing number of channels, the kinetic scheme of Eqn. 4 has been found to be inaccurate. More complex channel state models are needed and these can now be derived from single channel recordings. This means that explicit differential equations for the state model have to be written and these usually cannot be collapsed into the compact form of the HH equations (Eqn. 2). This change in the model generally reflects subtle changes in the gating behavior of channels.

- The HH model assumes that the instantaneous current-voltage relationship of a channel is linear, i.e. that $I_i = G_i(V, t)(V - E_i)$. As discussed in the notes on channel permeation models, the current-voltage relationship does not necessarily take this linear form. Usually a more accurate instantaneous current voltage model is the Goldman-Hodgkin-Katz constant field equation:

$$I_i = (\text{const.}) m^p h^q V \frac{[C_{\text{inside}} e^{z_i F V / RT} - C_{\text{outside}}]}{e^{z_i F V / RT} - 1} \quad (5)$$

where m and h are HH variables as in Eqn. 2 and Eqn. 5 is substituted for the linear current voltage relationships in Eqn. 1. Equation 5 is most commonly used in modeling Ca^{2+} channels, because the large concentration ratio $C_{\text{out}}/C_{\text{in}}$ leads to strong rectification. In these notes, the linear form of the equation, i.e. Eqn. 1, will be used for simplicity of analysis.

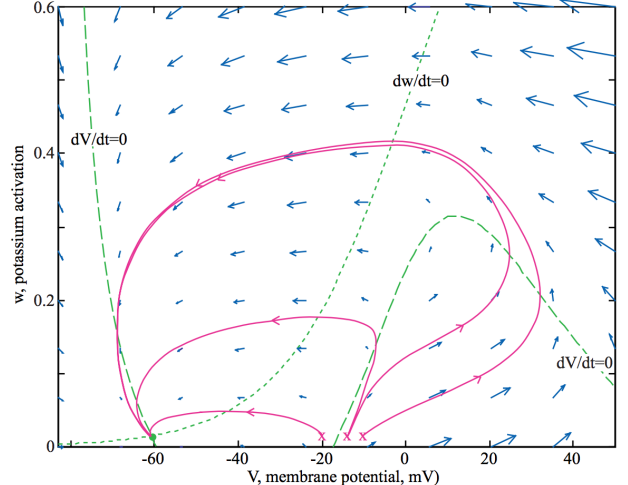


Fig. 5. Phase plane for the MLE with parameter set #1. The green dashed lines are the nullclines $dw/dt=0$ and $dV/dt=0$. The blue arrows show the directions and flow velocities of trajectories at the points corresponding to the tails of the arrows. The magenta solid lines are example trajectories for $V=-20$ mV, -14 mV, -13.9 mV, and -10 mV, respectively from left to right. The corresponding V versus time plots are shown in Fig. 6.

$$\frac{dV}{dt} = 0 \Rightarrow w_V(V) = \frac{I_{ext} - \bar{G}_{Ca} m_\infty(V)(V - E_{Ca}) - \bar{G}_L(V - E_L)}{\bar{G}_K(V - E_K)}$$

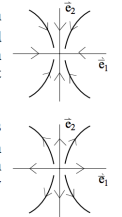
$$\frac{dw}{dt} = 0 \Rightarrow w_w(V) = w_\infty(V)$$

- Because a derivative is zero on a nullcline, the system is constrained to cross the nullclines moving either horizontally (across the $dw/dt=0$ nullcline) or vertically (across the $dV/dt=0$ nullcline). This can be seen in Fig. 5 by the directions of the arrows and the trajectories near the nullclines.
- The system's velocity changes direction across the nullclines. Thus, below the $dV/dt=0$ nullcline, the direction of flow along the V axis is positive, the blue arrows in Fig. 5 point to the right. Above the $dV/dt=0$ nullcline, the flow is to the left and the blue arrows point leftward. Similarly, below the $dw/dt=0$ nullcline, the flow is upward and above this nullcline, the flow is downward.

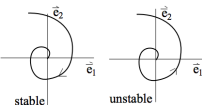
The differential equations for the HH parameters m , n , and h are parameterized by rate functions $A_x(t)$ and $B_x(t)$ where:

$$\begin{aligned} \frac{dm}{dt} &= A_m(V)[1 - m] - B_m(V)m & A_m(V) &= \frac{\alpha_m(V - V_{dm})}{1 - e^{(V - V_{dm})/K_{dm}}} & B_m(V) &= \beta_m e^{-(V - V_{bm})/K_{bm}} \\ \frac{dh}{dt} &= A_h(V)[1 - h] - B_h(V)h & A_h(V) &= \alpha_h e^{-(V - V_{ph})/K_{ph}} & B_h(V) &= \frac{\beta_h}{1 - e^{(V - V_{ph})/K_{ph}}} \\ \frac{dn}{dt} &= A_n(V)[1 - n] - B_n(V)n & A_n(V) &= \frac{\alpha_n(V - V_{nn})}{1 - e^{(V - V_{nn})/K_{nn}}} & B_n(V) &= \beta_n e^{-(V - V_{bn})/K_{bn}} \end{aligned} \quad (23)$$

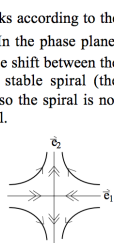
- 1. Stable node:** λ_1 and λ_2 both real and negative. In this case the exponentials in Eqn. 16 both decay with time, so the trajectories move smoothly and exponentially toward the equilibrium point. Such an equilibrium point is an attractor for trajectories in its vicinity and may be an attractor for a large part of the phase plane.



- 2. Unstable node:** λ_1 and λ_2 both real and positive. In this case the exponentials in Eqn. 16 both increase without bound, so the trajectories move away from the equilibrium point. The system is stable if placed exactly on such an equilibrium point, but any error will lead to a trajectory that moves away from the equilibrium point.



- 3. Stable and unstable spiral:** λ_1 and λ_2 both complex; complex eigenvalues must occur in complex conjugate pairs. There are two cases, a stable spiral occurs when the eigenvalues have a negative real part and an unstable spiral occurs when the eigenvalues have a positive real part. The solutions in this case take the form $Ae^{\text{Re}[\lambda]t} \cos(\text{Im}[\lambda]t + \theta)$. The cosine term gives an oscillation at frequency $\text{Im}[\lambda]/2\pi$ whose amplitude grows or shrinks according to the exponential multiplier $\exp(\text{Re}[\lambda]t)$. The sign of $\text{Re}[\lambda]$ determines which. In the phase plane, such solutions will spiral around the equilibrium point, since there is a phase shift between the time waveforms along \vec{e}_1 and \vec{e}_2 . The equilibrium point in Fig. 5 is a stable spiral (the exponential decay is faster than the period of the oscillation in this case, so the spiral is not seen; this case is very similar to a stable node) and Fig. 7 is an unstable spiral.



- 4. Saddle node:** one real positive eigenvalue and one real negative eigenvalue. The two exponential terms in Eqn. 16 now behave oppositely. One decays exponentially, the other grows exponentially. In the figure at right, λ_1 is negative, so the trajectories decay toward the equilibrium point along the direction of \vec{e}_1 ; λ_2 is positive, so the trajectories move away from the equilibrium point along \vec{e}_2 . Most trajectories follow a hyperbolic path, as sketched for the four trajectories shown with a single arrowhead. However, there are four trajectories which follow the directions of the eigenvectors \vec{e}_1 and \vec{e}_2 in the vicinity of the equilibrium point. These are indicated by the double arrowheads in the sketch. These trajectories are produced by initial conditions exactly on one of the eigenvectors, so that there is only one term in Eqn. 16.

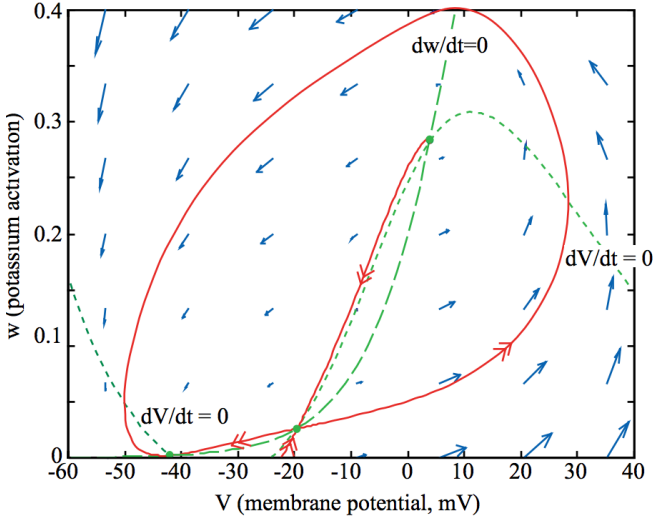


Fig. 8 Phase plane for the MLE with the parameters of set 2. All components are as for Fig. 5 except that the red lines are the stable and unstable manifolds. Note that there are now three equilibrium points (green dots).

1. The stable manifold running vertically downward from the saddle node acts as a true threshold for this system. This fact is apparent from Fig. 9. Consider trajectories from initial values (V_i, w_i) consisting of a depolarized membrane potential V_i and a resting value of the potassium channel state w_i . Such initial conditions lie along a line to the right of the resting potential. The two initial conditions marked with x's in Fig. 9 are on opposite sides of the stable manifold.

One gives a subthreshold return of membrane potential to rest and one gives an action potential, by following the rightward directed unstable manifold. In this case, initial values to the left of the manifold, by however small an amount, give subthreshold responses and initial values to its right give action potentials. Thus crossing the manifold is the condition for threshold in this system. Furthermore, unlike the action potentials shown in Fig. 5 for parameter set #1, the peak membrane potential of the action potential does not depend on the initial condition, because the action potential trajectories fall very close to the unstable manifold.

2. You should be able to convince yourself, from Fig. 8 and Fig. 9, that there is no limit cycle in this system. Because the membrane potential cannot cross any of the manifolds, there is no way to construct a loop in this phase space that is consistent with the blue arrows.

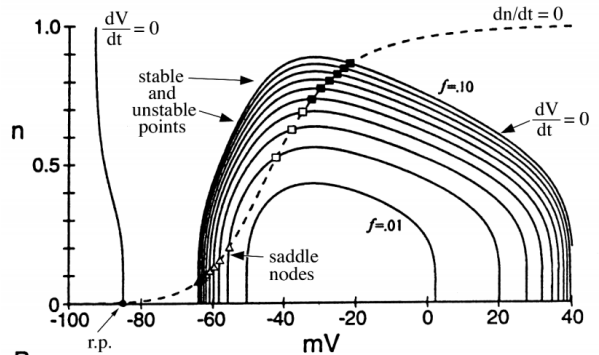
A sufficient condition for a limit cycle for order 2 systems (only) is provided by the Poincaré-Bendixson Theorem.

Theorem: Suppose that

1. R is a closed, bounded subset of the plane (shaded at right);
2. $d\vec{x}/dt = \tilde{f}(\vec{x})$ is a continuously differentiable vector field on an open set containing R ;
3. R does not contain any equilibrium points;
4. There exists a trajectory C that is confined in R , in the sense that it starts in R and stays in R for all time.

Then either C is a closed orbit (limit cycle) or it spirals toward a closed orbit as $t \rightarrow \infty$. In either case R contains a closed orbit.

A



B

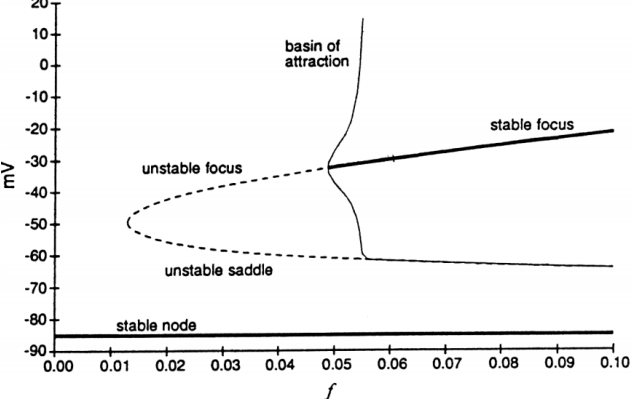
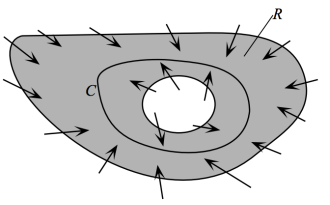


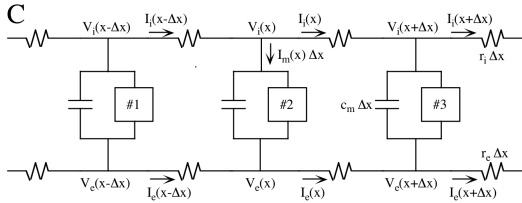
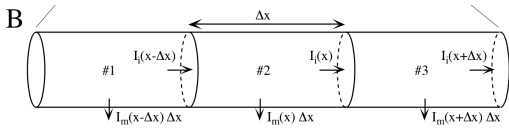
Fig. 17. A. Phase plane for the reduced Cannon et al. model with f varying from 0.01 to 0.1. Shown are nullclines; only the $dV/dt=0$ nullcline varies with f . Symbols marking equilibrium points vary in shape according to eq. point type. r.p. is equilibrium point at resting potential. B. Bifurcation diagram for this system. (modified from Fig. 10 of Cannon et al., 1998.)

Hopf bifurcation

There are several types of bifurcations, of which only the saddle-node variety has been mentioned. A common bifurcation seen in HH systems is a *Hopf bifurcation* which occurs when the eigenvalues of the linearization near an equilibrium point contain a complex conjugate pair. When the real part of the conjugate pair moves from negative (stable spiral) to positive (unstable spiral), the result is a Hopf bifurcation. The change from stable to unstable shown by the third eigenvalue in the reduced Cannon system (at $f=0.048$) is an example of a Hopf bifurcation. This is not a convenient example for discussion, because the typical bifurcation behavior (emergence of a limit cycle) is actually shown by the negative-time system in this case (i.e. the emergence of the unstable limit cycle). A detailed discussion of Hopf bifurcation can be found in Rinzel and Ermentrout (discussion of Fig. 7.2) and in Strogatz (pp. 248-254).



Derive non-linear cable equation



Ohm's law for current flow in the intracellular and extracellular spaces gives:

$$V_i(x) - V_i(x + \Delta x) = I_i(x) r_i \Delta x \quad \text{and} \quad V_e(x) - V_e(x + \Delta x) = I_e(x) r_e \Delta x$$

Rearranging and taking the limit as Δx goes to 0,

$$\lim_{\Delta x \rightarrow 0} \frac{V_i(x + \Delta x) - V_i(x)}{\Delta x} = \frac{\partial V_i}{\partial x} = -r_i I_i(x) \quad \text{and} \quad \frac{\partial V_e}{\partial x} = -r_e I_e(x)$$

Conservation of current at the intracellular and extracellular nodes gives

$$I_i(x - \Delta x) - I_i(x) = I_m(x) \Delta x \quad \text{or} \quad \frac{\partial I_i}{\partial x} = -I_m(x)$$

$$I_e(x - \Delta x) - I_e(x) = -I_m(x) \Delta x \quad \text{or} \quad \frac{\partial I_e}{\partial x} = I_m(x)$$

$$I_m(x) \Delta x = I_{ion}(x, V, t) \Delta x + c_m \Delta x \frac{\partial V}{\partial t}$$

$$\frac{\partial^2 V}{\partial x^2} = \frac{\partial^2 (V_i - V_e)}{\partial x^2}$$

$$= -r_i \frac{\partial I_i}{\partial x} + r_e \frac{\partial I_e}{\partial x}$$

$$= (r_i + r_e) I_m$$

nonlinear cable equation:

$$\frac{1}{r_i + r_e} \frac{\partial^2 V}{\partial x^2} = c_m \frac{\partial V}{\partial t} + I_{ion}$$

Parameters

$$r_i = \frac{R_i}{\pi a^2}$$

$$c_m = 2\pi a C$$

$$g_m = \frac{2\pi a}{R_m}$$

$$r_e = 0, \text{ assumed negligible}$$

$$\lambda = \sqrt{\frac{r_m}{r_e + r_i}} = \sqrt{\frac{r_m}{r_i}} = \sqrt{\frac{R_m a}{2 R_i}}$$

$$\tau_m = R_m C$$

$$G_\infty = \frac{1}{r_i \lambda}$$

$$\frac{\partial^2 \bar{V}}{\partial \chi^2} = (s + 1) \bar{V}$$

$$\left. \frac{\partial \bar{V}}{\partial \chi} \right|_{\chi=0} = -\frac{I_0}{s G_\infty} \quad \text{and} \quad v(\chi, T) < \infty \text{ for all } \chi, T$$

Equation 18 is now an ordinary differential equation whose solution takes the form

$$\bar{V}(\chi, s) = A(s) e^{\sqrt{s+1}\chi} + B(s) e^{-\sqrt{s+1}\chi} \quad (19)$$

where $A(s)$ and $B(s)$ are to be determined from the boundary conditions. Using the boundary condition at 0,

$$\begin{aligned} \left. \frac{\partial \bar{V}}{\partial \chi} \right|_{\chi=0} &= \left[\sqrt{s+1} A(s) e^{\sqrt{s+1}\chi} - \sqrt{s+1} B(s) e^{-\sqrt{s+1}\chi} \right]_{\chi=0} \\ &= \sqrt{s+1} [A(s) - B(s)] = -\frac{I_0}{s G_\infty} \end{aligned} \quad (20)$$

Derive linear cable equation

$$\frac{1}{r_i + r_e} \frac{\partial^2 V}{\partial x^2} = c_m \frac{\partial V}{\partial t} + g_m v = c_m \frac{\partial V}{\partial t} + \frac{1}{r_m} v$$

$$\frac{\partial^2 V}{\partial x^2} = \frac{\partial^2 (V - E_{rest})}{\partial x^2} = \frac{\partial^2 v}{\partial x^2}$$

and

$$\frac{\partial V}{\partial t} = \frac{\partial (V - E_{rest})}{\partial t} = \frac{\partial v}{\partial t}$$

$$\frac{r_m}{r_i + r_e} \frac{\partial^2 v}{\partial x^2} = r_m c_m \frac{\partial v}{\partial t} + v \quad \text{or} \quad \lambda^2 \frac{\partial^2 v}{\partial x^2} = \tau_m \frac{\partial v}{\partial t} + v$$

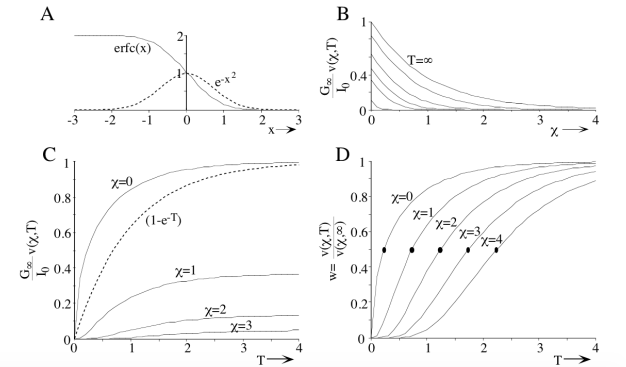
$$\frac{\partial^2 v}{\partial \chi^2} = \frac{\partial v}{\partial T} + v$$

$$v(\chi, T) = \frac{I_0}{2 G_\infty} \left\{ e^{-\chi} \operatorname{erfc} \left[\frac{\chi}{2\sqrt{T}} - \sqrt{T} \right] - e^{\chi} \operatorname{erfc} \left[\frac{\chi}{2\sqrt{T}} + \sqrt{T} \right] \right\} \quad (24)$$

The function $\operatorname{erfc}(x)$ is the complementary error function, defined as

$$\operatorname{erfc}(x) = 1 - \frac{2}{\sqrt{\pi}} \int_0^x e^{-\xi^2} d\xi \quad (25)$$

Figure 5A shows plots of $\exp(-x^2)$ and $\operatorname{erfc}(x)$ for reference; erfc is a standard function and algorithms for computing it are found in Matlab and other mathematics programs.



3 points refer to previous plots

1. Figure 5C shows plots of the growth of membrane potential in response to the step current injection; each curve shows potential growth at a different position along the cylinder, as labeled. Note that at $\chi=0$ the potential grows to a steady value relatively quickly. The growth is faster than exponential, as seen by the comparison with the function $(1-\exp(-T))$, which is plotted for comparison. As the point moves away from the end of the cable (larger χ), the growth of potential is delayed and the steady state value of potential is smaller. The difference in growth rate can be seen in Fig. 5D where the same plots are shown, except normalized by their maximum value. Note that the membrane time constant τ_m sets the time scale of the response, in that the abscissae of Figs. 5C and 5D are scaled in units of τ_m .

Figure 5C illustrates the basic features of electrotonic conduction: as the potential spreads from the site of a disturbance (in this case the current injection at the end of the cable), the amplitude of the potential gets smaller and its time course is extended. In this case, the rise of the potential is delayed and its rise is slower.

2. Figure 5B shows the potential spread along the cylinder at various times following the onset of the current at $T=0$. The most illuminating case is for $T=\infty$, i.e. in the steady state. In the steady state, Eqn. 24 becomes

$$v(\chi, T \rightarrow \infty) = \frac{I_0}{G_\infty} e^{-\chi/\lambda} = \frac{I_0}{G_\infty} e^{-x/\lambda} \quad (26)$$

This equation illustrates the meaning of the space constant λ . The decay of potential is exponential along the cylinder, so that potential decays by 1/e for every distance λ . Thus the space constant is a measure of how far a disturbance spreads away from the point of current injection.

Equation 26 also allows the meaning of the parameter G_∞ to be understood. Note that at $\chi=0$, $v(T=\infty)=I_0/G_\infty$. Thus the resistance looking into the end of the semi-infinite cylinder in the steady state, for application of D.C. current, is $1/G_\infty$. This is the basis for the statement made earlier that G_∞ is the input conductance of a semi-infinite cable.

3. A measure of the speed of electrotonic spread can be gotten from the points marked by black circles in Fig. 5D. These circles mark the times at which the potential is half its steady state value, for different values of χ . If the χ values are plotted against the half-times, the result is a straight line with slope $2\lambda/\tau_m$ (Jack et al., 1975). This value can be thought of as the speed of spread of electrotonic disturbances. Of course, it is not a true propagation speed, in the sense of the action potential propagation speed, because there is no fixed waveshape that is propagating, i.e. this is not a true wave. Nevertheless, this speed provides a way to calculate the time delays expected in electrotonic conduction. Note that it varies as the square root of the cylinder radius, since

$$\text{speed} = 2 \frac{\lambda}{\tau_m} = \sqrt{\frac{2a}{R_m R_i C^2}} \quad (27)$$

Rall motorneuron model

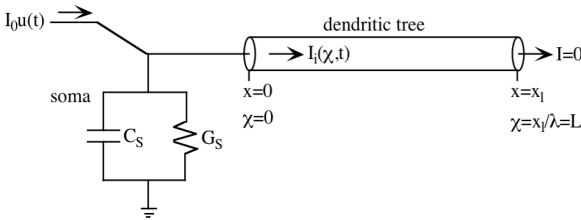


Figure 6. Rall motorneuron model. The soma is represented by the point-model consisting of the somatic capacitance C_s and resting conductance G_s . The dendritic tree is represented by a single membrane equivalent cylinder, which runs from $x=0$ to $x=x_i$. L is the **electrotonic length** of the dendritic cable. $I_0 u(t)$ is an external current injected into the soma of the cell through a microelectrode.

$$\begin{aligned} \left. \frac{\partial v}{\partial \chi} \right|_{\chi=L} &= 0 \\ I_0 u(t) &= C_S \left. \frac{\partial v}{\partial t} \right|_{\chi=0} + G_S v(\chi=0, T) - G_\infty \left. \frac{\partial v}{\partial \chi} \right|_{\chi=0} \\ &= \frac{C_S}{\tau_m} \left. \frac{\partial v}{\partial T} \right|_{\chi=0} + G_S v(\chi=0, T) - G_\infty \left. \frac{\partial v}{\partial \chi} \right|_{\chi=0} \end{aligned}$$

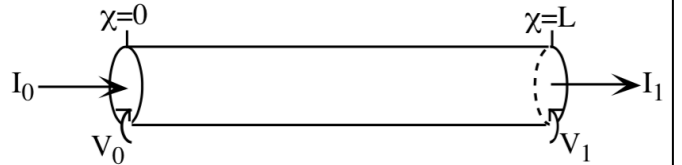


Figure 7. Two-port model for a length of dendritic cylinder

$$\begin{aligned} v(\chi=0, T) &= V_0(T) \quad \text{and} \quad v(\chi=L, T) = V_1(T) \\ I_i(\chi=0, T) &= I_0(T) \quad \text{and} \quad I_i(\chi=L, T) = I_1(T) \end{aligned}$$

There must also be a boundary condition in the time dimension. One of three situations will be considered. In each case, the cable equation is reduced to the ordinary differential equation

$$\frac{d^2 \bar{V}}{d\chi^2} = q^2 \bar{V} \quad (31)$$

where q is a variable that depends on the situation considered. The three situations are as follows:

- D.C. steady state:** in this case, all the sources are D.C. values and enough time has elapsed that the membrane potential and all currents in the system are steady, not varying with time. In this case $\partial v / \partial T = 0$ in Eqn. 10, $q=1$, and $\bar{V} = v$ in Eqn. 31.
- Laplace transform from zero initial conditions:** this is the same transform that was applied in Eqns. 15-18. In this case, $q = \sqrt{s+1}$ and $\bar{V}(\chi, s)$ is the Laplace transform of $v(\chi, T)$. The boundary conditions are also Laplace transformed.
- Fourier transform in the sinusoidal steady state:** this is similar to case 2. The sources are all sinusoidal at frequency ω and have been applied to the system long enough that transient components have died away. In this steady state, the membrane potentials and currents are also sinusoidal at frequency ω . Then, $q = \sqrt{1+j\omega}$, where $j = \sqrt{-1}$, and $\bar{V}(\chi, j\omega)$ is the Fourier transform of $v(\chi, T)$. The boundary conditions are also Fourier transformed in this case.

The solution to Eqn. 31 can be written as

$$\bar{V}(\chi, q) = A(q) \sinh(q\chi) + B(q) \cosh(q\chi) \quad (32)$$

where $\sinh(x) = [\exp(x) - \exp(-x)]/2$ and $\cosh(x) = [\exp(x) + \exp(-x)]/2$. It will also be useful to have the axial current $\bar{I}_i(\chi, q) = -G_\infty \partial \bar{V} / \partial \chi$ from Eqn. 14; from Eqn. 32, this is

$$\bar{I}_i(\chi, q) = -G_\infty q [A(q) \cosh(q\chi) + B(q) \sinh(q\chi)] \quad (33)$$

$$\bar{V}(0, q) = B \quad \bar{V}_0 \quad \text{and} \quad \bar{I}_i(0, q) = -G_\infty q A = \bar{I}_0 \quad (34)$$

A and B are determined by Eqn. 34, resulting in the following solution for membrane potential and axial current in the finite cable.

$$\begin{bmatrix} \bar{V}(\chi, q) \\ \bar{I}_i(\chi, q) \end{bmatrix} = \begin{bmatrix} \cosh(q\chi) & -\sinh(q\chi)/G_\infty q \\ -G_\infty q \sinh(q\chi) & \cosh(q\chi) \end{bmatrix} \begin{bmatrix} \bar{V}_0 \\ \bar{I}_0 \end{bmatrix} \quad (35)$$

Note that \bar{V}_1 and \bar{I}_1 are specified in this case by the functions in Eqn. 35 evaluated at $\chi=L$.

A second useful solution begins with an alternative way of writing the solutions to the cable equation, Eqn. 31:

$$\begin{aligned} \bar{V}(\chi, q) &= A(q) \sinh[q(L-\chi)] + B(q) \cosh[q(L-\chi)] \\ \bar{I}_i(\chi, q) &= G_\infty q \{ A(q) \cosh[q(L-\chi)] + B(q) \sinh[q(L-\chi)] \} \end{aligned} \quad (36)$$

In this case, applying the boundary conditions at $\chi=L$, i.e. \bar{V}_1 and \bar{I}_1 gives

$$\begin{bmatrix} \bar{V}(\chi, q) \\ \bar{I}_i(\chi, q) \end{bmatrix} = \begin{bmatrix} \cosh[q(L-\chi)] & \sinh[q(L-\chi)]/G_\infty q \\ G_\infty q \sinh[q(L-\chi)] & \cosh[q(L-\chi)] \end{bmatrix} \begin{bmatrix} \bar{V}_1 \\ \bar{I}_1 \end{bmatrix} \quad (37)$$

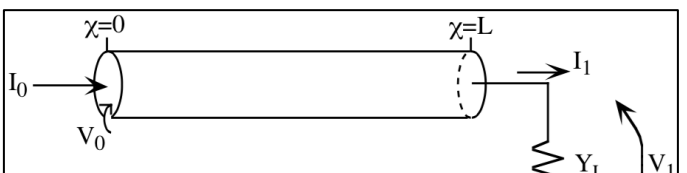


Figure 8. Finite cable loaded with an admittance Y_L at one end and voltage clamped at the other.

$$\begin{bmatrix} \bar{V}(\chi, q) \\ \bar{I}_i(\chi, q) \end{bmatrix} = \begin{bmatrix} \cosh[q(L-\chi)] & \sinh[q(L-\chi)]/G_\infty q \\ G_\infty q \sinh[q(L-\chi)] & \cosh[q(L-\chi)] \end{bmatrix} \begin{bmatrix} \bar{V}_i \\ Y_L \bar{V}_i \end{bmatrix} \quad (38)$$

The constraint that $\bar{V}(\chi=0, q) = \bar{V}_0$ can be applied to solve for \bar{V}_i , the one unknown in Eqn. 38. Using the voltage equation in Eqn. 38 gives

$$\bar{V}_0 = \bar{V}(\chi=0, q) = \bar{V}_i \left(\cosh qL + \frac{Y_L}{G_\infty q} \sinh qL \right) \quad (39)$$

Using Eqn. 39 to eliminate \bar{V}_i in Eqn. 38 gives the membrane potential in this finite cylinder as

$$\bar{V}(\chi, q) = \bar{V}_0 \frac{\cosh[q(L-\chi)] + \frac{Y_L}{G_\infty q} \sinh[q(L-\chi)]}{\cosh qL + \frac{Y_L}{G_\infty q} \sinh qL} \quad (40)$$

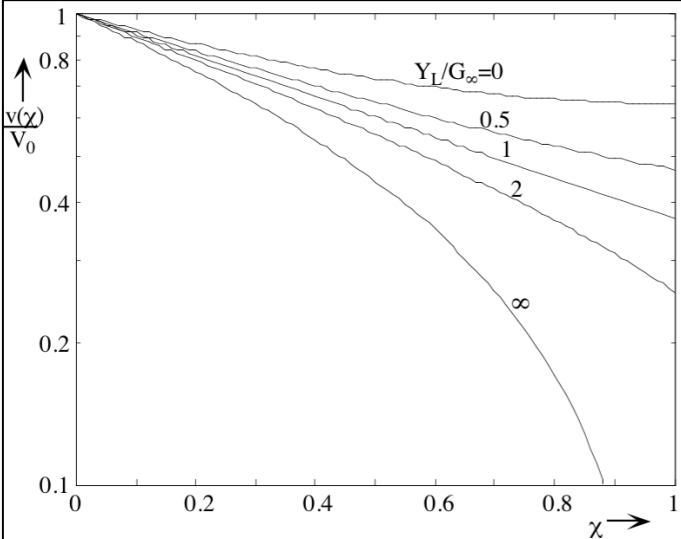
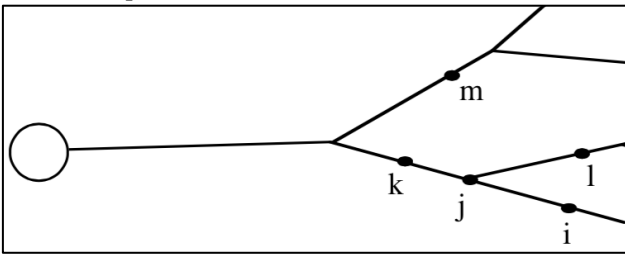


Figure 9 Decay of potential in a finite cylinder of electrotonic length 1 for the D.C. steady state case. Cylinder is voltage clamped at one end and terminated by a load admittance Y_L at the other (Fig. 8). Parameters on the curves are load admittance values relative to G_∞ .

The following are the three rules for determining relationships between currents injected at different points.



Rule 1: voltage transfer ratio This situation has already been analyzed. It is diagrammed in Fig. 8. What is desired is the voltage gain from V_0 to V_i in the presence of a load admittance Y_L . From Eqn. 39,

$$A_{0i} = \frac{\bar{V}_i}{\bar{V}_0} = \frac{1}{\cosh qL + \frac{Y_L}{G_\infty q} \sinh qL} \quad (40)$$

The gain A_{0i} is transformed in the same way as the voltages and currents. That is, if the situation is the D.C. steady state, then A_{0i} is the D.C. voltage ratio, a real number; if the cable equation has been Laplace transformed from 0 initial conditions, then A_{0i} is the complex transfer gain, a function of s .

This rule expresses the spread of voltage in the tree. For example, in Fig. 10, if \bar{V}_i is known, then \bar{V}_j , \bar{V}_k , etc. can be computed by application of Eqn. 40 (assuming that Y_L can be computed, the method for doing this is described below) either once or several times. Note that care must be taken to follow the direction of signal flow. If there is a source (voltage clamp or current injection) at point i then the voltage gains A_{ij} , A_{ik} , and A_{il} are meaningful because they follow the causal direction of signal flow, whereas A_{ji} is not, because it applies when a source at point j is producing a voltage at point i .

Rule 2: input admittance This rule also applies to the situation in Fig. 8, except the goal is to compute the input admittance $Y_{in} = \bar{I}_0/\bar{V}_0$ at one end of a cylinder loaded with admittance Y_L at the other end. The calculation is done directly from Eqn. 38, evaluated at $\chi=0$:

$$\begin{bmatrix} \bar{V}_0 \\ \bar{I}_0 \end{bmatrix} = \begin{bmatrix} \bar{V}(0, q) \\ \bar{I}_i(0, q) \end{bmatrix} = \begin{bmatrix} \cosh qL & \sinh qL/G_\infty q \\ G_\infty q \sinh(qL) & \cosh(qL) \end{bmatrix} \begin{bmatrix} \bar{V}_i \\ Y_L \bar{V}_i \end{bmatrix} \quad (41)$$

The input admittance is then the ratio of the two equations in Eqn. 41:

$$Y_{in} = \frac{\bar{I}_0}{\bar{V}_0} = G_\infty q \frac{\sinh qL + \frac{Y_L}{G_\infty q} \cosh qL}{\cosh qL + \frac{Y_L}{G_\infty q} \sinh qL} = G_\infty q \frac{\tanh qL + \frac{Y_L}{G_\infty q}}{1 + \frac{Y_L}{G_\infty q} \tanh qL} \quad (42)$$

A special case of importance is when $Y_L=0$, which is usually assumed at the end of a dendritic tree. In this case,

$$Y_{in} = G_\infty q \tanh qL \quad (43)$$

The second rule allows computation of the input admittance of any point on a dendritic tree. The computation is done constructively, as illustrated in Fig. 11. Consider the problem of

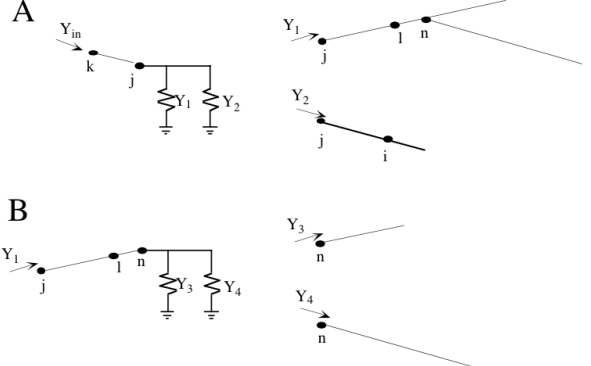


Figure 11 Illustrates the decomposition of the dendritic tree of Figure 10 in order to compute the input admittance at point k , looking out toward the end of the tree. A first segment of the tree, from k to j , terminated by input admittances of the two branches connected to j , shown at right. B Second segment, computing Y_1 , the input admittance at j looking out the branch toward l and n .

computing the input admittance, looking out toward the end of the dendrites, at point k on the dendritic tree of Fig. 10. As shown in Fig. 11A, this is the input admittance of the cable from k to j terminated by the parallel combination of admittances Y_1 and Y_2 . These are the input admittances of the two branches at j , shown at right in Fig. 11A. Admittance Y_2 can be computed immediately from Eqn. 43, because it is the input admittance of a single cable terminated at the end of the tree. Admittance Y_1 requires another decomposition, shown in Fig. 11B. At point n there are two branches, with input admittances Y_3 and Y_4 . Both of these can be computed immediately from Eqn. 43. Once Y_3 and Y_4 are computed, Y_1 can be computed from Eqn. 42 using Y_3+Y_4 as the load admittance for the cable shown in the left part of Fig. 11B. Now the input admittance at k can be computed from Y_1 and Y_2 using Eqn. 42 and the cable in the left part of Fig. 11A.

Note that the input admittance at a point on the tree can be computed using this rule, by summing the input admittances looking away from the point in the two directions, toward and away from the soma.

Rule 3: transfer impedance The third rule allows calculation of the potential produced at a point by current injected at a different point. The situation is diagrammed in Fig. 12. A current \bar{I}_{inj}

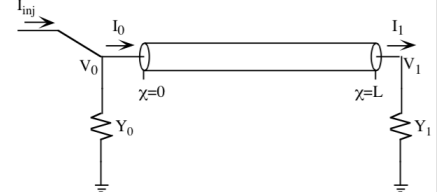


Figure 12 Cable terminated at both ends by admittances and driven at one end by an injected current.

is injected at one end of a cylinder and a potential \bar{V}_1 is produced at the other end. The relationship between these two can be computed by starting with Eqn. 35, evaluated at $\chi=L$. With the constraints provided by the load impedance at the right end and the current injection at the left end, the equation gives

$$\begin{bmatrix} \bar{V}_1 \\ \bar{I}_1 \bar{V}_1 \end{bmatrix} = \begin{bmatrix} \cosh(qL) & -\sinh(qL)/G_\infty q \\ -G_\infty q \sinh(qL) & \cosh(qL) \end{bmatrix} \begin{bmatrix} (\bar{I}_{inj} - \bar{I}_0)/Y_0 \\ \bar{I}_0 \end{bmatrix} \quad (44)$$

If \bar{I}_0 is eliminated between the two equations in Eqn. 44, that leaves an equation relating \bar{I}_{inj} and \bar{V}_1 . The transfer impedance K_{01} is the ratio of these two quantities and is given by

$$K_{01} = \frac{\bar{V}_1}{\bar{I}_{inj}} = \frac{1}{(Y_0 + Y_1) \cosh qL + \left(\frac{Y_0 Y_1}{G_\infty q} + G_\infty q \right) \sinh qL} \quad (45)$$

The combination of transfer impedance and voltage transfer ratio can be used to compute transfer impedances between any two points in a dendritic tree. For example, for the tree in Fig. 10, if a current is injected at point i , the voltages at various other points on the tree will be given by Equations 46. Note how the branch points are handled. The transfer impedance K_{ij} cannot extend across a branch point, so the transfer impedance and voltage gain must be applied sequentially from branch point to branch point.

$$\begin{aligned}\bar{V}_j &= K_{ij} \bar{I}_{inj} & \bar{V}_k &= K_{ij} A_{jk} \bar{I}_{inj} \\ \bar{V}_l &= K_{ij} A_{jl} \bar{I}_{inj} & \bar{V}_n &= K_{ij} A_{jn} A_{ln} \bar{I}_{inj}\end{aligned}\quad (46)$$

These relationships use Rules 1 and 3 explicitly; they also require Rule 2, however, in order to compute the admittances necessary to the use of Rules 1 and 3.

Symmetry: $K_{ij} = K_{ji}$

Positivity: $K_{ij} \leq K_{ii}$ and $K_{ij} \leq K_{jj}$ (for D.C. steady state ($q=1$ and all quantities real) only). The quantities K_{ij} and K_{jj} are the input impedances (resistances in the D.C. steady state) of the dendritic tree at points i and j .

Transitivity: $K_{ij} = K_{il} K_{lj} / K_{ll}$ True for points i , l , and j on a path without loops and point l in between i and j .

Equivalent cylinder theorem. Consider an arbitrarily branching structure like the tree shown in Fig. 15. Three conditions can be stated:

1. The cumulative electrotonic lengths from soma to the tip of the dendritic tree is the same by all direct paths. That is, for the example in Fig. 15

$$L_{total} = L_{11} + L_{21} + L_{31} = L_{11} + L_{21} + L_{32} = \dots = L_{11} + L_{22} + L_{34} \quad (47)$$

2. At every branch point, there is an impedance match in the sense that the sum of the G_∞ s of the child branches equals the G_∞ of the parent branch. For example

$$G_{\infty 11} = G_{\infty 21} + G_{\infty 22} \quad \text{and} \quad G_{\infty 21} = G_{\infty 31} + G_{\infty 32} \quad \text{etc.} \quad (48)$$

Note that this is usually stated as the 3/2 power law: at every branch point

$$a_{parent}^{3/2} = \sum_{\text{all child branches } j} a_j^{3/2} \quad (49)$$

3. The termination condition is the same at all dendritic tips, in the sense that $Y_{ij} / qG_{\infty ij}$ is the same for all terminal branches.

If these conditions are true, then the dendritic tree is equivalent to a cylinder with the electrotonic length L_{total} , a G_∞ value equal to $G_{\infty 11}$, and terminated by an admittance which is the sum of the admittances terminating the original tree. The equivalence holds in the following ways:

1. If the soma is voltage (or current) clamped, then $v(\chi)$ is the same in the original tree and the equivalent cylinder. Note that this rule applies to voltage measured in terms of electrotonic distance χ , not physical distance x .
2. The input admittance of the original tree is the same as that of the equivalent cylinder.
3. If current I_{inj} is injected into one branch at an electrotonic length L_i from the soma in the original tree, then the potential distribution is the same in the original tree and cylinder for the ultimate parent branch only. For example, if current were injected into branch 21 or 33 in the tree in Fig. 15, then the potential would be the same in the 11 branch and in the first L_{11} of the equivalent cylinder.

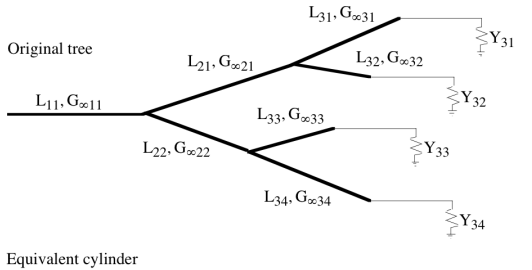


Figure 15 Top shows the branching structure of a dendritic tree with arbitrary termination admittances. Bottom shows the equivalent cylinder for this tree. L is electrotonic length equal to physical length divided by length constant. G is the infinite cylinder input conductance, Eqn. 13. Y is the admittance terminating each dendritic branch.

$$\frac{1}{r_i+r_e} \frac{\partial^2 V}{\partial x^2} = i_m(x,t,V) = \text{membrane current/unit length of cylinder}$$

$$\frac{1}{r_i+r_e} \frac{\partial^2 \bar{V}}{\partial x^2} = \bar{i}_m(x,j\omega,V)$$

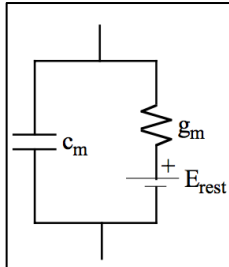
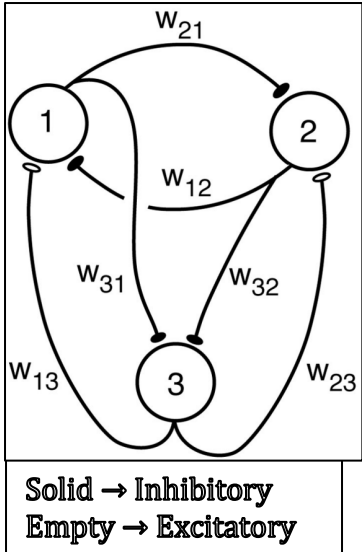
and

$$\bar{i}_m(x,j\omega,V) = \frac{1}{z_m} \bar{V}$$

where the bars indicate that the variables have been Fourier transformed.

$$\frac{1}{r_i+r_e} \frac{\partial^2 \bar{V}}{\partial x^2} \approx \frac{1}{r_i} \frac{\partial^2 \bar{V}}{\partial x^2} = \frac{1}{z_m} \bar{V} \quad \text{or} \quad \frac{z_m}{r_i} \frac{\partial^2 \bar{V}}{\partial x^2} - \bar{V} = 0$$

All following notes about cable theory are extra, taken from the solutions to homework 6 and 7.



From circuit model shown at left, we require that:

1. Assume that V is the output (no spikes)
2. g_m is linear, $E_m = E_{rest} = 0$
3. $I_{sym} = s [\sum w_i V_i]$, where s is a squashing fn, i.e.

$$s = \frac{1}{1+e^{-x}}$$

Perceptron

$$V = s [\vec{w} \cdot \vec{u}]$$

$$V(t \rightarrow \infty) = \begin{cases} 1, & \vec{w} \cdot \vec{u} \geq \gamma \\ -1, & \vec{w} \cdot \vec{u} < \gamma \end{cases}$$

Where u is input, and w is weight, and γ is a learned constant

3-layer perceptron can solve any continuous mapping function

4-layer perceptron can solve any mapping

Supervised Learning (differentiable $s(x)$)

Patterns: $\vec{u}^1, \dots, \vec{u}^p$

Desired outputs: $\vec{v}^1, \dots, \vec{v}^p$

$$Err[\vec{w}] = \frac{1}{2} \sum_p (v^p - s(\vec{w} \cdot \vec{u}^p))^2$$

$$\frac{\partial Err}{\partial w_k} = - \sum_p [v^p - s(\vec{w} \cdot \vec{u}^p)] \left. \frac{\partial s}{\partial h} \right| \vec{u}_k^p$$

Where $h = \vec{w} \cdot \vec{u}^p$

$$\nabla Err = \left[\frac{\partial Err}{\partial w_1}, \dots, \frac{\partial Err}{\partial w_k} \right]$$

Gradient Descent

$$\Delta \vec{w} = -\epsilon \vec{\nabla} Err$$

Hebbian (unsupervised) Learning

$$\tau \frac{dV}{dt} = -V + \vec{w} \cdot \vec{u}$$

$$\Delta \vec{w} = \frac{1}{\tau_w} V \vec{u} = \frac{1}{\tau_w} \langle V \vec{u} \rangle$$

$$\|\Delta \vec{w}\|^2 \approx \frac{2}{\tau_w} V^2 > 0$$

Weights can unboundedly grow... so Oja's Rule is req'd:

$$\Delta \vec{w} = \frac{1}{\tau_w} [V \vec{u} - V^2 \vec{w}]$$

Hopfield Nets

$$\tau = -S_i + F \left[\sum_i w_{ij} x_j \right]$$

Assume Steady State for analysis \rightarrow discrete steps from $\vec{S} \rightarrow \vec{S}'$
 F can be any fn ($sign()$, for instance)

$\vec{S}' = \vec{S}$ is a stable state. Patterns are stable states.

For patterns ξ :

$$\vec{\xi}^j = \{\xi_1^j, \dots, \xi_N^j\}, j = 1 \rightarrow P$$

$$w_{ij} = \frac{1}{N} \sum_{k=1}^N \xi_i^k \xi_j^k$$

Where $w_{ii} = \frac{P}{N}$; $w_{ij} = w_{ji}$

Noisy patterns require more signal than noise for the pattern to be recovered consistently.